Diamond & Related Materials 166 (2026) 113711

Contents lists available at ScienceDirect

Diamond & Related Materials

journal homepage: www.elsevier.com/locate/diamond

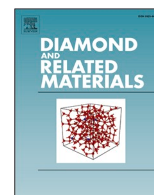

Electron-beam induced modulation of surface conduction in hydrogen-terminated diamond

Sebastian Wood [a,c,*], Evgheni Strelcov [b], Junyeob Song [b], Albert Davydov [a], Jabez J. McClelland [b], Andrei Kolmakov [b]

[a] Material Measurement Laboratory, National Institute of Standards and Technology (NIST), Gaithersburg, MD, 20899, United States
[b] Physical Measurement Laboratory, National Institute of Standards and Technology (NIST), Gaithersburg, MD, 20899, United States
[c] Electromagnetic and Electrochemical Technologies Department, National Physical Laboratory (NPL), Hampton Road, Teddington, Middlesex, TW11 0LW, United Kingdom

ARTICLE INFO

Keywords:
Hydrogen terminated diamond
Electron beam
Surface conductivity
KPFM
UV
EBIC

ABSTRACT

Hydrogen-terminated diamond is a promising platform for diamond-based high-power-frequency electronics and radiation-hardened semiconductor devices exhibiting controllable electrical conduction through an accumulated sub-surface 2D hole-gas layer. The diamond conductivity is highly sensitive to local surface conditions, offering new opportunities for device engineering, quantum sensors, and switches, as well as presenting a challenge for device stability. Here we study the impact of focused electron-beam exposure on hydrogen-terminated transfer-doped diamond, revealing a reversible loss of local conductivity. Using Kelvin probe force microscopy (KPFM), we show that irradiation leads to a local change in surface potential and find that both ultra-violet (UV) light and ambient exposure can act to restore the conductivity. We propose that the electron beam injects negative sub-surface charge into deep trap states that electrostatically gate the local hole transport. In some cases, local electron-stimulated desorption of electron-accepting surface species may also contribute.

1. Introduction

Diamond exhibits attractive properties for high-performance power and high-frequency electronic devices: high intrinsic carrier mobilities for both electrons and holes, high thermal conductivity, and superior mechanical and radiation hardness [1]. The ultra-wide bandgap of around 5.5 eV makes intrinsic diamond an excellent electrical insulator with a high breakdown field. However, whilst the material properties of diamond lead to attractive figures-of-merit for high-power and high-frequency semiconductor devices, the actual performance achieved is frustrated by efforts to dope the material. The introduction of boron or phosphorus as *p*- and *n*-type dopants, respectively, suffers from high activation energies, and impurity-related scattering reduces the charge carrier mobilities achieved. However, surface transfer doping, *e.g. via* diamond surface hydrogenation, has emerged as an attractive alternative to bulk doping. Hydrogenating the diamond surface: a) induces negative electron affinity at the surface and b) removes oxygen atoms, which pin its Fermi level. Consequently, the unpinned Fermi level can be bent upwards by a variety of adsorbed electron-accepting species (surface transfer doping) [1–3], or electrostatic gating (accumulation channel devices) [4–7], resulting in formation of a high mobility 2D hole-gas (2DHG) below the surface of the diamond. Since initial demonstrations of H-terminated diamond field effect transistors (FETs), progress has focused on understanding the mechanisms and engineering of controllable surface transfer doping using solid-state electron-acceptors or dielectrics to enable gate-doping [8,9].

A key challenge for H-terminated diamond (HD) devices is the stability of the surface transfer doping. This is especially relevant to proposed applications in harsh environments where elevated temperatures and exposure to ionizing radiation are known to impact the surface stability and conductivity [10–12]. Additionally, these effects can also be exploited in device nanofabrication, using thermal processing and electron-beam (e-beam) lithography to define device structures with nanoscale resolution or control surface functionalisation [13,14]. Nanoscale imaging, characterization and modification of HD surfaces is possible with microscopic techniques, such as scanning probe (SPM) and scanning electron (SEM) microscopies. Several reports published over the last two decades focused on using both techniques to oxidize and

* Corresponding author at: Electromagnetic and Electrochemical Technologies Department, National Physical Laboratory (NPL), Hampton Road, Teddington, Middlesex, TW11 0LW, United Kingdom.
E-mail address: sebastian.wood@npl.co.uk (S. Wood).

https://doi.org/10.1016/j.diamond.2026.113711
Received 28 February 2026; Received in revised form 17 April 2026; Accepted 4 May 2026
Available online 5 May 2026
0925-9635/© 2026 The Authors. Published by Elsevier B.V. This is an open access article under the CC BY-NC-ND license (http://creativecommons.org/licenses/by-nc-nd/4.0/).

image HD surfaces [15–17]. Kelvin probe force microscopy (KPFM), an SPM technique, was used to measure contact potential difference (CPD) between the oxygenated and hydrogenated diamond [15,16,18,19]. However, these studies were conducted in ambient conditions and, therefore, suffered from uncontrolled surface adsorbates, which affected both measured CPD and surface conductivity. The aim of this study was to explore the effect of electron-beam exposure on the HD surface using an *in situ*, *in vacuo* combination of scanning electron microscopy (SEM), KPFM, and electrical measurements in a controllable way. We find that the e-beam exposure causes a loss of surface conductivity associated with a temporary local reduction in surface potential (negative charge injection). Furthermore, we show that ultra-violet (UV) irradiation or atmospheric exposure results in a recovery of conductivity, indicating that the disruption of the 2DHG is associated with both local trapping of charge and desorption of electron-accepting species. Using electron beam-induced current (EBIC) measurements [20,21] to study this effect, it is demonstrated that in some conditions, the e-beam induced gating can be reversed using UV irradiation without atmospheric exposure. These results and the multimodal method demonstrated are important for efforts to improve the stability of HD for harsh operating conditions, and for optimisation of e-beam lithography for HD device fabrication.

2. Methods

2.1. Sample preparation

The sample was a single-crystal chemical vapor deposition (CVD) grown diamond (3.0 mm × 3.0 mm, thickness 0.25 mm). The specified boron concentration was <0.05 μmol/mol and nitrogen concentration < 1 μmol/mol, the top surface was {100} polished with a quoted roughness, $R_a < 30$ nm. Prior to defining an electrical channel, the surface of the diamond sample was hydrogenated in a commercial 2.5 kW microwave (2.45 GHz) plasma reactor. The sample was first chemically cleaned *via* boiling in a mixture of sulfuric and nitric acids (1:1 L/L ratio) for 30 min. The sample was thoroughly rinsed in DI water, followed by ethanol, and N_2 dried before placing it onto a polycrystalline diamond wafer in the plasma reactor. In the reactor, the sample was heated in pure hydrogen plasma (12,000 Pa) to *ca.* 700 °C to 800 °C by ramping the plasma forward power, held for *ca.* 5 min, and then slowly cooled still under the plasma conditions. After hydrogenation, the sample was exposed to air, which activates the surface conductivity through the transfer-doping *via* the adsorption of ambient species. The typical sheet resistance of such HD is on the order of 10 kΩ per square. The electrode structure (Fig. 1(a)) with thin electrical channels was lithographically defined by thermally depositing gold (ohmic) electrodes (80 nm thick) with a pair of gold pads connected by a single gold strip. Note that when electron lithography was used, care was taken to avoid e-beam penetration to the bare diamond during the writing process. In the centre of the Au strip the width was reduced to around 3 μm. The rest of the gold was dissolved in 2.5 g:10 g:100 g I_2:KI:water solution. After final photoresist removal and cleaning in isopropanol, the sample was mounted on the SPM sample holder using silver paste and attaching thin wires between the gold pads and the contact terminals on the sample holder. The sample was then subjected to an oxygen plasma treatment (*ca.* 30 Pa, 20 W for 10 min) in order to oxidize the bare areas (Oxygen-terminated diamond, OD) whilst protecting the H-termination under the gold track. The processes for hydrogen-termination and oxygen-termination closely match those reported elsewhere in literature and verified using photoemission spectroscopy [22,23]. The strong contrast in secondary electron emission and surface potential exhibited below demonstrate the overall efficacy of these surface treatments.

The oxygen plasma treatment was also used to remove organic residues from the sample and the sample holder in order to prevent them from re-depositing onto the sample and changing the measured CPD. An exposed channel of H-terminated diamond was opened using a 0.5 μm radius tungsten needle on a micromanipulator to peel off a small section of the gold. The resulting break was roughly 5 μm long and can be seen in the optical and SEM images in Fig. 1. This step was performed in air immediately prior to transferring the sample to the SEM load-lock. The tungsten needle was cleaned by ultrasonication in isopropyl alcohol and acetone prior to use to minimise contamination of the sample and the weak adhesion of gold on the diamond surface causes the metal to peel

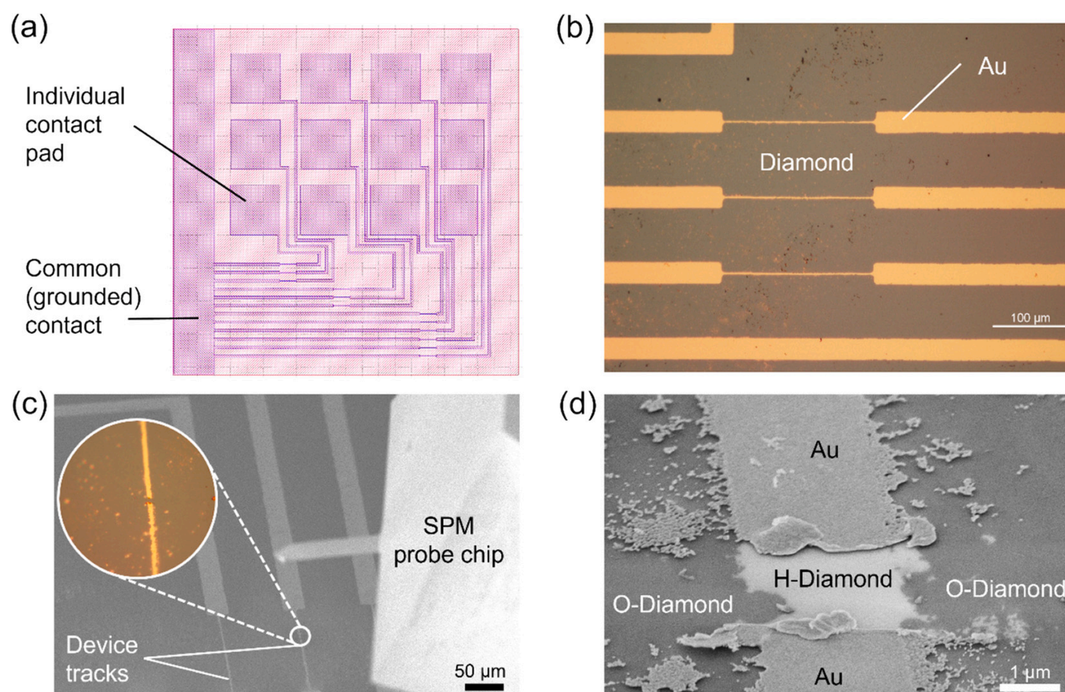

Fig. 1. (a) Schematic diagram of the sample showing the layout of the Au contacts. (b) An optical micrograph shows the detail of microscopic Au tracks on the diamond surface. (c) SEM image showing parallel device tracks and the SPM probe chip above the sample; the inset shows an optical image of a break in the Au track defining the HD device channel. (d) SEM image showing detail of the sample, including the break in the Au track exposing HD surrounded by OD.

away easily. This method was found to preserve a much cleaner H-terminated diamond surface than a wet iodide etch of the gold.

The sample for EBIC measurements was prepared using the same CVD diamond material and techniques, but with a larger (100 μm × 600 μm) HD strip. This allowed for the direct landing of microprobes and eliminated the need for separate electrical contact pads.

2.2. SEM-KPFM

An instrument combining SEM and SPM in one vacuum chamber was used for characterization. Pt/Ir-coated SPM tips were used throughout, with an indicative resonance frequency of 310 kHz. The SPM tip (on its holder) and tweezers were also cleaned with oxygen plasma prior to mounting in the SEM, and the SEM chamber itself was plasma cleaned to minimise carbon contamination on the sample during measurements.

The SEM vacuum level was 7.3×10^{-5} Pa, and SEM images were recorded using an In-Lens secondary electron detector, a beam voltage of 5 kV, a working distance of 10.1 mm, and a 50 pA beam current. E-beam damage tests were performed using a line-scanning mode. The 50 pA beam current was used throughout, but various beam voltages (2 kV, 5 kV, and 15 kV), exposure times, and scanning line lengths were used.

SEM imaging was used for positioning the SPM probe on the sample. E-beam exposure was minimised during measurement set-up to avoid adventitious carbon deposition and to help isolate the e-beam-induced effects under study. The SPM probe can be seen in the SEM images presented in Fig. 1. Note that the sample and SPM hardware are tilted at 60° with respect to the SEM beam, and therefore, the perspective of the SEM images differs from the AFM images.

KPFM was performed using the single-pass mode to record both topography and contact potential difference (CPD) signals simultaneously. The tip oscillation frequency was offset to −70% from the resonance peak amplitude (around 309 kHz). For the Kelvin probe signal, a sinusoidal electrical bias with a frequency of 93 kHz and an amplitude of 3 V was applied to the tip.

SEM images are presented with no additional processing. KPFM data was post-processed using a custom-written code to correct for distortions arising from scanner imperfections. Polynomial flattening and scar-removal was applied to topography images, for CPD scar correction was applied but no flattening [24].

2.3. Electrical measurements

In situ electrical measurements were performed using a computer-controlled source-meter unit with feedthroughs on the SEM chamber to connect to the sample.

2.4. UV exposure

A low-pressure mercury lamp was used to expose the sample to UV light (254 nm main emission line) positioned approximately 1 cm from the sample to provide a nominal intensity of 5 mW·cm^{-2} for a duration of 5 min. This required transferring the sample to an argon-filled glovebox using a vacuum-tight sample transfer shuttle. The glovebox had <1 ppm of oxygen and water, but the leak rate in the transfer shuttle was not measured.

2.5. EBIC

EBIC measurements were performed using an SEM with a pair of micromanipulated electrical probes and a current amplifier to record the signal. No electrical bias was applied to the current-collecting probe, and the other probe was grounded. For these experiments, the electron beam energy was set to 2 kV, and the primary beam current was in the 50 pA to 250 pA range. The above UV source was mounted at the load-lock of the SEM chamber so the sample could be exposed to UV light without breaking the vacuum. Note that the mercury lamp also has an appreciable intensity at 185 nm that is capable of initiating band-to-band transitions and corresponding photocurrent in the diamond sample. For the charge de-trapping EBIC experiments, the irradiated sample was moved *in vacuo* to the load-lock and irradiated by UV light for 2 min. The sample to source distance was 2 mm.

3. Results & discussion

Since the gold etching solution can contaminate the surface, the H-terminated channel was exposed by locally peeling-off part of the Au-capped track with a clean needle just prior to loading the sample into the SEM chamber. The SEM image of Fig. 1(d) clearly shows the broken Au track with an approximate width of 3 μm. The Au etch process results in line-edge roughness at this scale, but the pattern of the removed Au is clearly visible in the secondary electron image since the HD exhibits strongly enhanced emission compared with the surrounding OD. Bright secondary electron emission arises from the negative electron affinity that permits low-energy secondary electrons to escape easily from the HD surface [25]. Exposure to the e-beam was minimised at this stage, but some exposure was inevitable to position the AFM probe over the region of interest.

KPFM measurements on the exposed HD track prior to the e-beam exposure experiments are presented in Fig. 2(a) and (b). The topography map shows minimal contrast between the OD and HD regions with a step height of <1 nm. However, the CPD map shows a strong contrast, with a mean CPD value of 338 mV ± 52 mV for the OD and 580 mV ± 32 mV for the HD (taking the mean and standard deviation of CPD for the respective areas). This indicates that the work function of the OD is around 240 mV larger than the work function of the HD, which is consistent with other reports using KPFM [18,19]. The absolute work function values cannot be reliably extracted because the work function of the tip is subject to variation during measurements. We note that other reports on this work function difference using photoelectron spectroscopy exhibit larger differences up to 2 eV [26]. Such methods benefit from ultra-high vacuum conditions to preserve surface cleanliness, whereas the KPFM measurements are highly sensitive to adsorbed species on both the sample surface and the probe tip. The edges of the HD region in the CPD map appear less sharply defined than in the topography map. This may simply arise from the expected lower spatial resolution of the KPFM measurement, but raises the possibility of whether it is possible to measure the lateral charge distribution associated with the junction between the HD and OD regions [27]. To study the impact of e-beam exposure, the SEM beam was used to irradiate a line with a nominal length of 5 μm cutting across the full width of the HD channel using a beam voltage of 5 kV for a duration of 360 s. Based on the 50 pA beam current, this indicates a dose of 3.6 nC·μm^{-1}. The electrical current through the device was measured during the exposure by applying a constant bias of 50 mV across the channel. The current-time measurement is plotted in 2(c) and shows an immediate increase in current for the duration of the exposure, which can be understood as electron-beam induced generation of charge pairs [28]. Additionally there is a gradual reduction in the current during exposure indicating an increase in channel resistance, which persists beyond the exposure period and is followed by an ongoing reduction in current over a period of several minutes. The drop in current from 52 nA to 39 nA after 1000 s represents a 25% decrease. Reduction in conductivity during exposure could be rationalised in terms of prior reports as electron-beam-induced oxidation of the HD surface or of adsorbed electron-accepting species [25,29]. However, this cannot explain the continued reduction in current beyond the end of exposure, which is more consistent with charge-induced effects [30,31].

Repeating the KPFM measurement immediately after exposure reveals no significant change in the topography (Fig. 2(d)), but a clear linear feature in the CPD (Fig. 2(e)) corresponding with the e-beam exposure is observed. The full extent of this effect is more clearly appreciated with a larger area CPD map of the sample shown in Fig. 3(a).

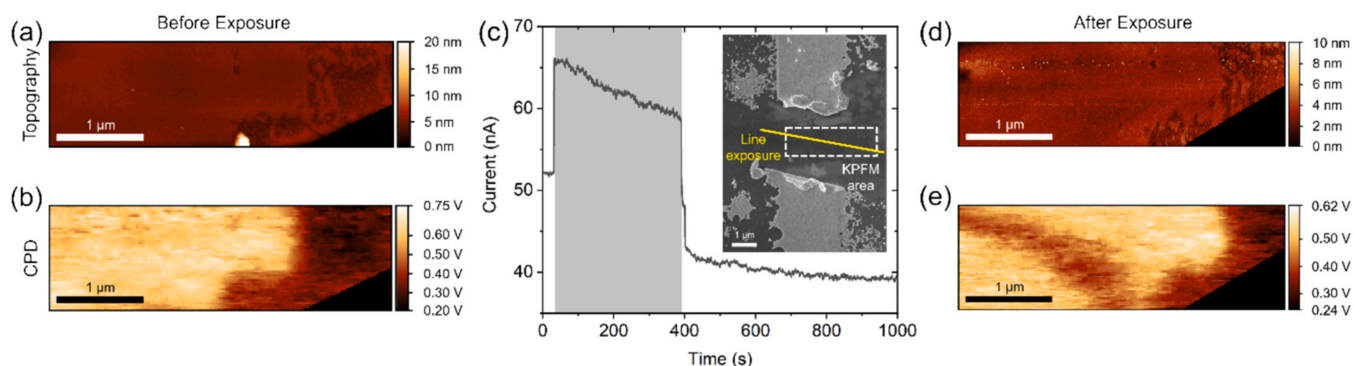

Fig. 2. (a) Topography and (b) CPD maps for the region of interest e-beam exposure. (c) Current-time measurement with applied bias of 50 mV across the device channel with the shaded region indicating the 360 s duration of 5 kV e-beam exposure of a 5 μm line across the HD channel. Inset indicates the approximate positions of the region of interest for the KPFM measurements (white dashed outline) and the linear e-beam exposure (yellow line). Note that this normal-incidence measurement was performed at the end of the experiments and shows reduced secondary electron emission from the HD region (d) Topography, and (e) CPD maps for the region of interest after e-beam exposure. Missing data from KPFM are masked in black.

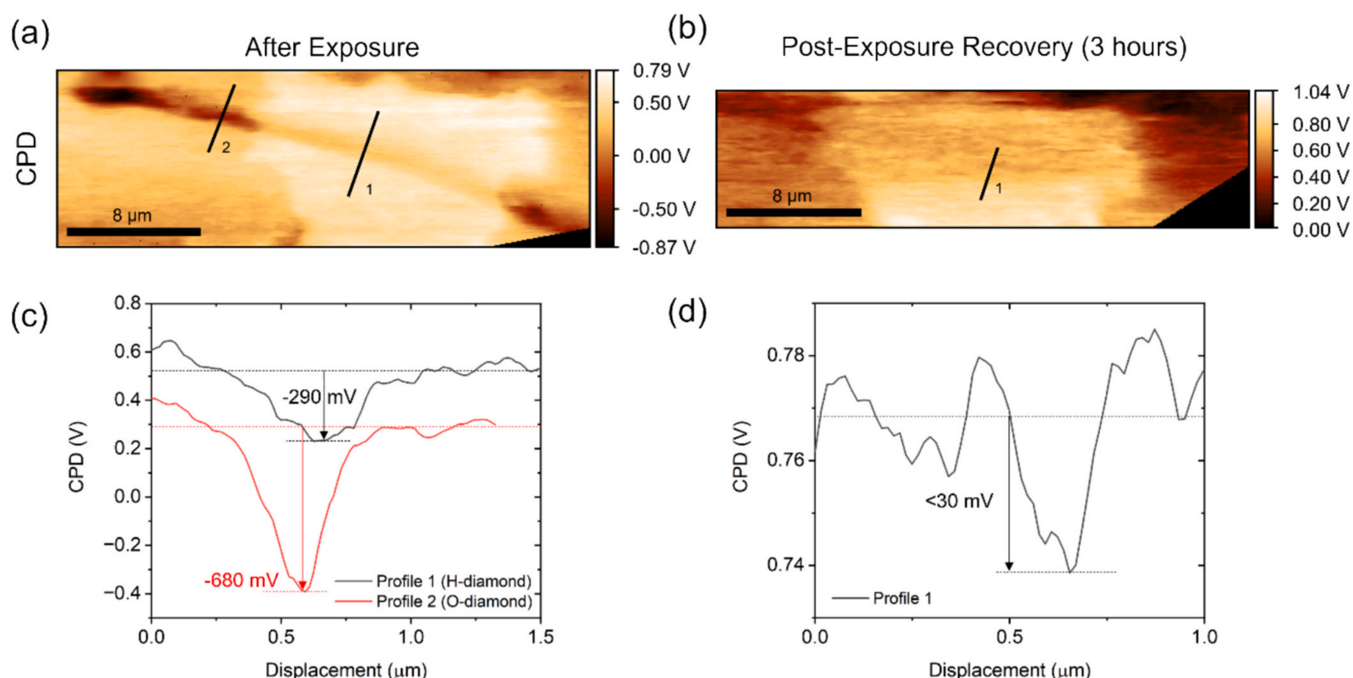

Fig. 3. CPD measurements of the HD region of interest (a) after exposure to the e-beam, and (b) approximately 3 h later. Missing data from KPFM are masked in black. (c) CPD profiles extracted from (a) indicating the local dip in CPD associated with the beam exposure comparing the HD and OD regions. (d) CPD profile extracted from (b) showing almost complete loss of contrast after 3 h recovery. Note the difference in scale on axes between (c) and (d).

Here, the dark line is seen to extend across the full width of the HD channel as well as the OD regions on either side. In both cases, the CPD is locally reduced, but the magnitude of the effects varies, as shown by the linear profiles plotted in Fig. 3(c). For the OD, the electron-beam induced reduction in CPD has over double the magnitude compared to the HD (*ca.* 680 mV compared with *ca.* 290 mV). In both cases, the width of the linear feature is around 300 nm (full-width at half-maximum), which is clearly much larger than the spatial resolution of the CPD measurement, indicating the spatial extent of the effect.

The observed reduction in CPD could be explained by three different effects:

1. e-beam induced carbon deposition,
2. e-beam induced surface oxidation or desorption of surface species,
3. implantation of negative charge under the surface.

Effect 1, carbon deposition, was mitigated by plasma-cleaning of the chamber, sample, sample holder, and SPM probe holder immediately prior to the experiment. In addition, deposited amorphous carbon should have a work function similar to that of OD, and we would therefore expect a smaller CPD contrast for carbon deposition on OD than on the HD. However, the opposite is observed in Fig. 3(c). Furthermore, carbon deposition would be non-reversible, so it is ruled out by the discussion below.

To discriminate between effects 2 and 3, the sample was kept in the SEM chamber without beam exposure and the KPFM scan was repeated roughly 3 h later. The result, presented in Fig. 3(b) shows that the linear feature is no longer present, though we note that there was no corresponding recovery in the electrical conductivity. The CPD profile extracted from the region, plotted in Fig. 3(d) shows that any residual contrast is less than 30 mV on the HD region. If the observed CPD contrast were associated with a chemical change in the sample surface

(oxidation of the diamond or desorption of acceptor species) we would expect it to persist under these conditions [32]. Rather, the transience of the feature is more consistent with local charging of the surface that dissipates gradually. In this case, the lower CPD signal associated with the e-beam exposure is indicative of negative charging of the sample. This contrasts with the expectation that the high secondary electron yield of HD leads to positive charging of the surface, but can be rationalised by the relatively high beam voltage (5 kV), as well as the fact that the KPFM measurement is performed several minutes after the e-beam exposure, which could allow surface positive charges to dissipate whereas more deeply trapped negative charges persist [25,31,33–35]. The smaller magnitude of the local charging effect on the HD compared with the OD could be attributed to a combination of a higher secondary electron emission yield (lower electron affinity) and the higher surface conductivity. The spatial broadening of the linear feature can be understood as the lateral migration of charge carriers under the local electric field or defocusing of the e-beam caused by surface charging [36]. We also note that space charge effects can have a significant effect in considering the complex interaction of the electron beam with the material sub-surface [37].

To explore the electron-beam-induced effect further, different exposure times (10 s, 60 s, 360 s, corresponding to higher charge dose) and beam voltages (2 kV, 5 kV, 15 kV, corresponding to deeper charge implantation) were tested on the same device. The results are plotted in Fig. 4. The measurements were conducted sequentially with periods of several hours between exposures to allow the current to stabilise. In each case, the current-time measurement has a similar form with a step-wise increase and decrease in the measured current when the e-beam exposure starts and ends, along with a more gradual decrease in current over several minutes after the exposure. However, for the shortest duration exposure (10 s) the current after the exposure remains higher than the initial current for around 100 s and stabilises close to the original level. In contrast, for longer exposures (60 s and 360 s), there is a clear downward trend in the current both during and after the exposure, with overall decreases in current of approximately 9% and 16% respectively, after 1000 s. This clearly shows that the magnitude of the effect depends on the dose of exposure, where increased duration of exposure results in a greater reduction in current. In each case, the continued decrease in current over a period of minutes after the exposure period is consistent with a local charging effect, as identified by the KPFM measurement above. Negative charge is locally injected and continues to redistribute during and after exposure. We propose that this injected charge becomes implanted in the insulating bulk of the diamond substrate and gates the near-surface conductive channel. Subsequently, this charge dissipates slowly, partially neutralizes the charge, but also distributes it more evenly over a larger area. This results in the gating of a wider region of the conductive channel and therefore a decreasing current. We have observed a similar gating effect by the injected charge in the accumulation channel HD transistor devices, where charge dissipation in a vacuum took days. Interestingly, for the 10 s exposure, the current is slightly enhanced after exposure. This could be due to either a small baseline drift (trapped injected charge contributing directly to the measured current as it gradually de-traps), or to the generation of additional acceptor species by the e-beam (*e.g.* water molecule radiolysis with the formation of OH^{-} groups on the surface). In addition to the gating effect, the reduction in current caused by the longer duration could indicate desorption of electron-accepting species. The observation that the charge-related CPD signal recovers but the electrical conduction does not require that the conductive channel is sensitive to a low concentration (below the CPD detection limit) of trapped charges persisting for long durations, or that there is an additional effect such as desorption of electron-accepting species.

Comparing the effect of beam voltages with a fixed exposure time (360 s) also gives qualitatively similar current-voltage plots with increased current during exposure and a subsequent slow decay of current towards a lower level. The percentage drop in current at the end of the measurement in each case is approximately 24% (2 kV), 25% (5 kV), and 9% (15 kV), suggesting that penetration of the higher energy e-beam deeper into the surface has a reduced impact on the conductive channel. This is consistent with the understanding that the HD conduction is located close to the surface.

The results so far demonstrate an e-beam induced modulation of

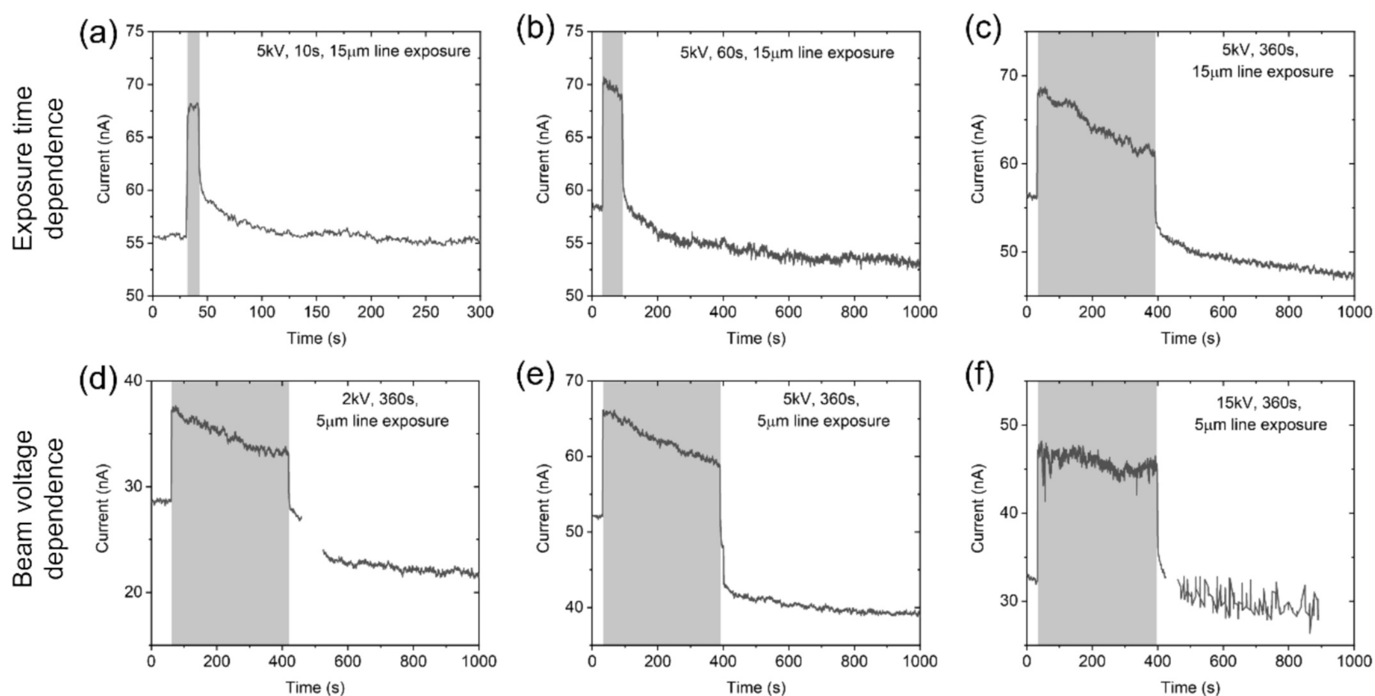

Fig. 4. Current-time measurements of the HD channel conductivity (50 mV applied bias) comparing exposure times: (a) 10 s, (b) 60 s, (c) 360 s each at 5 kV with a 15 μm exposure line; and comparing beam voltages: (d) 2 kV, (e) 5 kV, (f) 15 kV, each for 360 s with a 5 μm exposure line. Note that the initial current is different in each case due to the sequential exposure and partial recovery.

current through the HD device channel associated with both an accumulation of negative charges that dissipates over a matter of hours, and a longer-lived increase in the channel resistance. However, the relationship between these observations is unclear. Specifically, whether the injected negative charge is responsible for gating the 2DHG channel, or whether it arises from an associated effect such as desorption of electron-accepting surface species, or partial oxidation of the HD surface [2,29,38]. To test this, the e-beam exposed sample was illuminated with UV light under inert (dry nitrogen) conditions, which would be expected to facilitate de-trapping of charge. This required transferring the sample to a glovebox without ambient exposure, so a controlled experiment was performed by measuring the resistance of the device before and after transfer to the glovebox, as well as after exposure to UV light. At the end of the experiment the sample was exposed to air as a final test. The results are plotted in Fig. 5(a).

Immediately prior to the electron-beam measurements the resistance was measured as 278 kΩ (instrument-based uncertainties are below 1 Ω), though we note that the sample had already been exposed to the beam for initial SEM imaging. The resistance increased to 715 kΩ at the end of the e-beam measurement campaign. After transferring the sample to the argon-filled glovebox in a vacuum-tight shuttle, the resistance dropped to 470 kΩ, which indicates some level of exposure to relevant conditions inherent in the transfer process and glovebox environment. After exposure to the mercury vapor lamp for 5 min the resistance dropped further to 170 kΩ, and then exposing to ambient air at the end of the study the resistance decreased slightly more to 156 kΩ. This sequence indicates that both exposure to the mercury lamp emission and exposure to atmospheric conditions result in a substantial recovery of the conduction. The mercury lamp was used because the UV emission lines could optically de-trap charges in the device, though the visible light contributions were not excluded in this experiment [18]. Additionally, UV light could desorb surface acceptor species, increasing resistivity. Thus, the overall effect would be a combination of the two mechanisms with opposite effects. Air exposure, on the other hand, could increase acceptor adsorbate coverage, which is required to generate the 2DHG in HD [1,39].

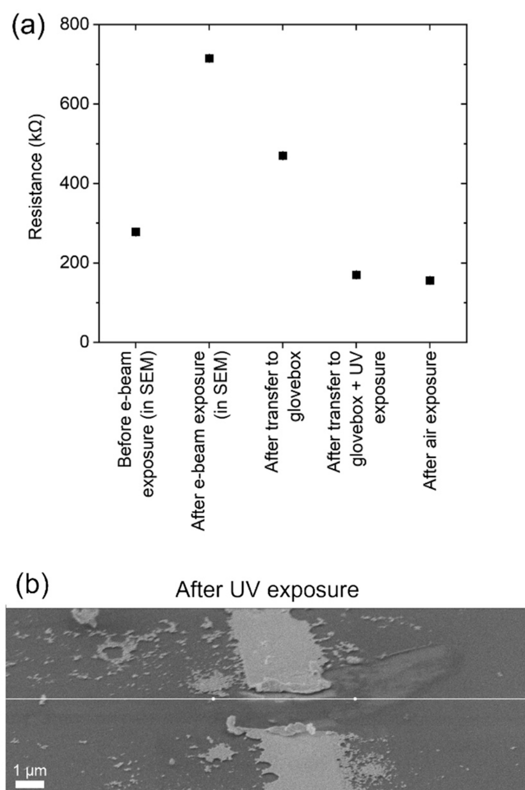

Fig. 5. (a) Electrical resistance of the device before and after the e-beam exposure study, comparing the effects of exposure to glovebox transfer chamber, UV exposure, and ambient exposure. (b) SEM image of the sample measured after exposure to the UV light, showing no recovery of bright secondary electron emission for the HD region.

A repeated SEM measurement of the sample after atmospheric exposure showed that the bright secondary electron emission from the HD region was no longer observed – see Fig. 5(b). This indicates a permanent change in the sample surface resulting from a combination of e-beam, UV, and air exposure, but the full recovery of electrical conduction demonstrates that the surface's hydrogen-termination remains. Rather, the reduced secondary electron emission yield is interpreted as surface contamination during argon and air exposure since adventitious carbon deposition has been ruled out [40]. The fact that atmospheric exposure is required to restore the surface conductivity suggests that electron-accepting surface adsorbates have been lost during e-beam exposure.

Further verification of the proposed mechanism of e-beam-induced gating of the 2DHG arising from local charge injection was obtained using EBIC measurements to map the collection of e-beam-induced charges from an HD. In this case, the HD region was a 600 µm long strip surrounded by OD and contacted with electrical probes at the ends, as shown in Fig. 6(a) SEM image. Again, the bright contrast of the HD region in SEM is due to its negative electron affinity that sponsors the secondary electron emission. The EBIC map of the sample in Fig. 6(b) shows a strong hole-collecting signal and a gradual resistor-like potential drop across the strip, indicating high conductivity and absence of the electroactive defects or interfaces. After that, the central square part of the strip was locally e-beam exposed (2 kV, 20 s) with an approximate dose of 5 fC·µm^{-2}. The subsequent EBIC map shows the appearance of the electroactive defect that impedes the hole transport from the right part of the HD strip towards the collecting electrode (Fig. 6(c)). Interestingly, the very border of the irradiated region has even darker contrast compared to the rest of the HD channel. This is presumably due to the appearance of the local embedded electric field that inhibits the recombination of the electron-hole pairs. The latter corroborates with the accumulation of the locally trapped negative charge that causes local band bending and sponsors e-h pairs dissociation. We observed that this EBIC map remains stable, provided the probing e-beam current remains in the picoampere range. The sample was then exposed to UV irradiation with the Hg lamp connected to the SEM load-lock for a duration of 2 min. Re-measuring the sample with EBIC after this exposure shows a recovery of the original state with minimal gradient in the EBIC signal along the HD strip, as shown in Fig. 6(d). In this experiment, the vacuum was not broken for UV exposure and therefore confirms that (at least under these exposure conditions) the e-beam induced gating can be assigned to localised injection and trapping of the charge that can be de-trapped or neutralized using UV excitation.

4. Conclusions

Drawing together the experimental results, we propose the following description for the effect of e-beam exposure on HD diamond. During exposure to the beam, electron-hole pairs, injected electrons, and uncompensated holes contribute directly to the current measured through the HD channel under bias. The e-beam causes the injection and trapping of negative charge into the insulating diamond substrate bulk, which persists under vacuum conditions. Gradual de-trapping and redistribution of this charge continues to affect the measured current for a period of minutes to hours, and gates the 2DHG. The e-beam exposure also contributes negatively to the conductivity of the HD by desorption or decomposition of electron-accepting adsorbates from the sample. The hydrogen-termination itself remains intact. Exposure to light and atmospheric conditions causes a recovery of the hole-gas conduction channel through re-absorption of electron-accepting species and light-

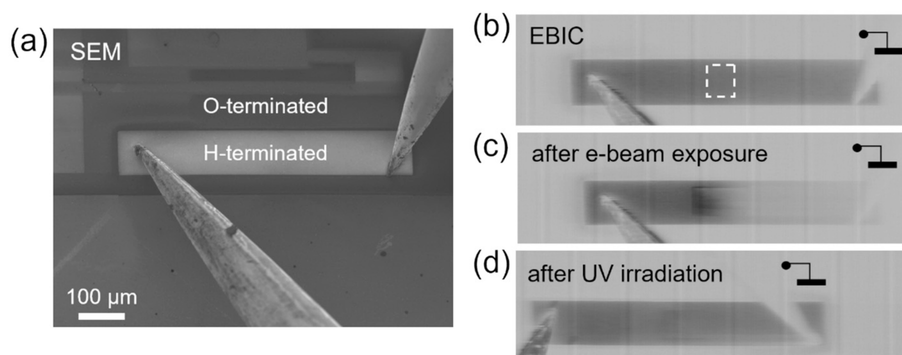

Fig. 6. (a) SEM image showing HD strip surrounded by OD and contacted with electrical probes. (b) EBIC image (primary beam parameters: 2 keV, 70 pA) mapping collection of e-beam-induced current from HD region. The right-hand probe was grounded, and current was collected from the left probe. The white rectangle indicates the region of the following extended e-beam exposure (2 keV, 250 pA, 20 s). (c) EBIC map following exposure of the central region. (d) EBIC map of the same region after exposure to UV irradiation for 2 min.

induced de-trapping of injected charge. Further study is required to quantitatively discriminate the relative magnitudes of the trapped charge and desorption of surface species on the gating of the 2DHG conduction channel, but the EBIC measurements show that UV irradiation can reverse the gating without atmospheric exposure.

These findings are relevant to the proposed use of e-beam lithography for the fabrication of HD devices, where the detailed interaction of the beam with the material is critical to achieve the highest writing resolution. The demonstrated effect of the injection of charge is expected to reduce the spatial resolution, so careful resist engineering must be taken to avoid e-beam penetration into the diamond. It is also reported elsewhere that the e-beam oxidizes the diamond surface, but the results presented here show that this is not necessarily the case.

The effects of ionizing radiation on HD are also relevant to its potential applications in harsh environments, such as use in space, nuclear reactors, and radioactive sites, where the radiation hardness of electronic devices is required. The methods demonstrated here, using combined SEM, KPFM, and *in situ* electrical measurements, are ideally suited to detailed investigations of the irradiation of surfaces by high-energy electrons.

CRediT authorship contribution statement

Sebastian Wood: Writing – review & editing, Writing – original draft, Visualization, Methodology, Investigation, Funding acquisition, Formal analysis, Data curation. **Evgheni Strelcov:** Writing – review & editing, Writing – original draft, Visualization, Validation, Software, Methodology, Investigation, Conceptualization. **Junyeob Song:** Writing – review & editing, Investigation. **Albert Davydov:** Writing – review & editing, Supervision, Resources, Project administration. **Jabez J. McClelland:** Writing – review & editing, Validation, Supervision, Resources, Project administration, Methodology, Funding acquisition. **Andrei Kolmakov:** Writing – review & editing, Writing – original draft, Validation, Supervision, Resources, Project administration, Methodology, Investigation, Funding acquisition, Formal analysis, Conceptualization.

Declaration of competing interest

The authors declare that they have no known competing financial interests or personal relationships that could have appeared to influence the work reported in this paper.

Acknowledgements

This work was supported by the NPL International Secondment Scheme, and the UK Department for Science, Innovation and Technology (DSIT) through the National Measurement System and the International Science Partnerships Fund (ISPF) project “Setting the Standards for Semiconductors”. The authors are thankful to Dr. Stephen Moxim and Dr. Sergiy Krylyuk (at NIST) and Dr. Ben Reed (at NPL) for careful reading of the manuscript and useful suggestions, and to Dr. James E. Butler (Euclid Techlabs, LLC) for hydrogenation and Dr. Trey Diulus (NIST) for XPS/AES characterization of the diamond samples.

Data availability

Data will be made available on request.

References

[1] K.G. Crawford, I. Maini, D.A. Macdonald, D.A.J. Moran, Surface transfer doping of diamond: a review, Prog. Surf. Sci. 96 (1) (2021), https://doi.org/10.1016/j.progsurf.2021.100613.
[2] F. Maier, M. Riedel, B. Mantel, J. Ristein, L. Ley, Origin of surface conductivity in diamond, Phys. Rev. Lett. 85 (16) (2000) 3472–3475, https://doi.org/10.1103/PhysRevLett.85.3472.
[3] J. Ristein, Surface transfer doping of diamond, J. Appl. Phys. D Appl. Phys. 39 (2006) R71.
[4] J.A. Garrido, et al., The surface conductivity at the diamond/aqueous electrolyte interface, J. Am. Chem. Soc. 130 (12) (2008) 4177–4181, https://doi.org/10.1021/ja078207g.
[5] H. Kawarada, M. Aoki, M. Ito, Enhancement mode metal-semiconductor field effect transistors using homoepitaxial diamonds, Appl. Phys. Lett. 65 (12) (1994) 1563–1565, https://doi.org/10.1063/1.112915.
[6] Y. Sasama, et al., High-mobility p-channel wide bandgap transistors based on h-BN/diamond heterostructures, Nat. Electron. 5 (2022) 37–44, https://doi.org/10.1038/s41928-021-00689-4.
[7] C. Qu, I. Maini, Q. Guo, A. Stacey, D.A.J. Moran, Extreme enhancement-mode operation accumulation channel hydrogen-terminated diamond FETs with Vth < −6 V and high on-current, Adv. Electron. Mater. 11 (8) (2024) 2400770.
[8] M. Tordjman, Diamond electronics with high carrier mobilities, Nat. Electron. 5 (2022) 21–22.
[9] R. Alhasani, et al., An enhanced two-dimensional hole gas (2DHG) C–H diamond with positive surface charge model for advanced normally-off MOSFET devices, Sci. Rep. 12 (1) (2022) 1–10, https://doi.org/10.1038/s41598-022-05180-4.
[10] G. Speranza, et al., In situ thermal treatment of UV-oxidized diamond hydrogenated surface, Surf. Sci. 604 (9–10) (2010) 753–761, https://doi.org/10.1016/j.susc.2010.01.004.
[11] C. De Santi, et al., Reliability of H-terminated diamond MESFETs in high power dissipation operating condition, Microelectron. Reliab. 114 (2020) 113898.
[12] T. Masumura, et al., Irradiation effects of X-rays up to 3 MGy on hydrogen-terminated diamond MOSFETs, Diam. Relat. Mater. 135 (2023) 109825.
[13] V. Dergianlis, M. Geller, D. Oing, N. Wöhrl, A. Lorke, Patterning of diamond with 10 nm resolution by electron-beam-induced etching, Nanotechnology 30 (36) (2019), https://doi.org/10.1088/1361-6528/ab25fe.
[14] J. Liu, H. Ohsato, X. Wang, M. Liao, Y. Koide, Design and fabrication of high-performance diamond triple-gate field-effect transistors, Sci. Rep. 6 (September) (2016) 1–2, https://doi.org/10.1038/srep34757.
[15] B. Rezek, C.E. Nebel, Electronic properties of plasma hydrogenated diamond surfaces: a microscopic study, Diam. Relat. Mater. 15 (9) (2006) 1374–1377, https://doi.org/10.1016/j.diamond.2005.10.002.
[16] C. Toma, et al., Tip voltage controlled local modification of hydrogenated diamond surface with an atomic force microscope, Phys. Status Solidi Appl. Mater. Sci. 204 (9) (2007) 2920–2924, https://doi.org/10.1002/pssa.200776321.

[17] T. Wang, et al., Low voltage fabrication of sub-nanometer insulating layers on hydrogenated diamond, J. Appl. Phys. 110 (3) (2011) 034311, https://doi.org/10.1063/1.3615956.

[18] B. Rezek, C.E. Nebel, Kelvin force microscopy on diamond surfaces and devices, Diam. Relat. Mater. 14 (2005) 466–469.

[19] M. Tachiki, et al., Characterization of locally modified diamond surface using Kelvin probe force microscope, Surf. Sci. 581 (2–3) (2005) 207–212, https://doi.org/10.1016/j.susc.2005.02.054.

[20] S. Kono, T. Teraji, H. Kodama, A. Sawabe, Reprint of 'imaging of diamond defect sites by electron-beam-induced current', Diam. Relat. Mater. 63 (2016) 30–37, https://doi.org/10.1016/j.diamond.2016.01.020.

[21] D.S. Ashby, et al., Identification of localized radiation damage in power MOSFETs using EBIC imaging, Appl. Phys. Lett. 118 (20) (2021), https://doi.org/10.1063/5.0053892.

[22] M. Kubovic, M. Kasu, Enhancement and stabilization of hole concentration of hydrogen-terminated diamond surface using ozone adsorbates, Jpn. J. Appl. Phys. 49 (11) (2010) 110208, https://doi.org/10.1143/JJAP.49.110208.

[23] C. Njel, H.A. Girard, M. Frégnaux, D. Aureau, J.C. Arnault, In situ photoemission spectroscopies to reveal surface transfer doping on hydrogenated milled nanodiamonds, Carbon N. Y. 230 (July) (2024) 119668, https://doi.org/10.1016/j.carbon.2024.119668.

[24] D. Nečas, P. Klapetek, Gwyddion: an open-source software for SPM data analysis, Cent. Eur. J. Phys. 10 (2012) 181–188.

[25] A. Shih, J. Yater, P. Pehrsson, J. Butler, C. Hor, R. Abrams, Secondary electron emission from diamond surfaces, J. Appl. Phys. 82 (4) (1997) 1860–1867, https://doi.org/10.1063/1.365990.

[26] G. Wan, M. Cattelan, N.A. Fox, Electronic structure tunability of diamonds by surface functionalization, J. Phys. Chem. C 123 (7) (2019) 4168–4177, https://doi.org/10.1021/acs.jpcc.8b11232.

[27] N. Barrett, et al., Operando x-ray photoelectron emission microscopy for studying forward and reverse biased silicon p-n junctions, Rev. Sci. Instrum. 87 (5) (2016) 053703, https://doi.org/10.1063/1.4948597.

[28] E. Wang, et al., Secondary-electron emission from hydrogen-terminated diamond: experiments and model, Phys. Rev. Spec. Top. Accel. Beams 14 (11) (2011) 1–7, https://doi.org/10.1103/PhysRevSTAB. 14.111301.

[29] A. Stacey, S. Prawer, S. Rubanov, R. Akhvlediani, S. Michaelson, A. Hoffman, Temperature enhancement of secondary electron emission from hydrogenated diamond films, J. Appl. Phys. 106 (6) (2009), https://doi.org/10.1063/1.3224881.

[30] W. Shi, et al., Reversible writing of high-mobility and high-carrier-density doping patterns in two-dimensional van der Waals heterostructures, Nat. Electron. 3 (2020) 99–105.

[31] A. Hoffman, et al., Decay of secondary electron emission and charging of hydrogenated and hydrogen-free diamond film surfaces induced by low energy electrons, J. Appl. Phys. 91 (7) (2002) 4726–4732, https://doi.org/10.1063/1.1456944.

[32] R.D. Ramsier, J.T. Yates, Electron-stimulated desorption : principles and applications, Surf. Sci. Rep. 12 (6–8) (1991) 246–378.

[33] R. Hristu, et al., Surface charge and carbon contamination on an electron-beam-irradiated hydroxyapatite thin film investigated by photoluminescence and phase imaging in atomic force microscopy, Microsc. Microanal. 20 (2) (2014) 586–595, https://doi.org/10.1017/S1431927614000191.

[34] Z.J. Ding, C. Li, B. Da, J. Liu, Charging effect induced by electron beam irradiation: a review, Sci. Technol. Adv. Mater. 22 (1) (2021) 932–971, https://doi.org/10.1080/14686996.2021.1976597.

[35] H.J. Hopman, J. Verhoeven, P.K. Bachmann, H. Wilson, R. Kroon, Secondary electron emission measurements on synthetic diamond films, Diam. Relat. Mater. 8 (6) (1999) 1033–1038, https://doi.org/10.1016/s0925-9635(98)00451-8.

[36] T. Plecenik, et al., Direct creation of microdomains with positive and negative surface potential on hydroxyapatite coatings, Appl. Phys. Lett. 98 (11) (2011) 14–16, https://doi.org/10.1063/1.3567532.

[37] T. Schmidt, A. Sala, H. Marchetto, E. Umbach, H.-J. Freund, First experimental proof for aberration correction in XPEEM: resolution, transmission enhancement, and limitation by space charge effects, Ultramicroscopy 126 (2013) 23–32, https://doi.org/10.1016/j.ultramic.2012.11.004.

[38] J.D. Wnuk, S.G. Rosenberg, J.M. Gorham, W.F. Van Dorp, C.W. Hagen, D. H. Fairbrother, Electron beam deposition for nanofabrication: insights from surface science, Surf. Sci. 605 (3–4) (2011) 257–266, https://doi.org/10.1016/j.susc.2010.10.035.

[39] L. Barron, Molecular Light Scattering and Optial Activity, Cambridge University Press, 2004.

[40] T. Yamada, A. Kojima, A. Sawabe, K. Suzuki, Passivation of hydrogen terminated diamond surface conductive layer using hydrogenated amorphous carbon, Diam. Relat. Mater. 13 (4–8) (2004) 776–779, https://doi.org/10.1016/j.diamond.2004.01.019.